An insertional mutagenesis screen identifies genes that cooperate with *Mll-AF9* in a murine leukemogenesis model

Rachel J. Bergerson,[1] Lara S. Collier,[2] Aaron L. Sarver,[3] Raha A. Been,[1] Sanne Lugthart,[4] Miechaleen D. Diers,[1] Johannes Zuber,[5] Amy R. Rappaport,[5,6] Molly J. Nixon,[1] Kevin A. T. Silverstein,[3] Danhua Fan,[3] Anne-Francoise J. Lamblin,[3] Linda Wolff,[7] John H. Kersey,[1] Ruud Delwel,[4] Scott W. Lowe,[5,6,8] M. Gerard O'Sullivan,[9] Scott C. Kogan,[10] David J. Adams,[11] and David A. Largaespada[1]

[1]Department of Genetics, Cell Biology and Development and Department of Pediatrics, Masonic Cancer Center, University of Minnesota Twin Cities, Minneapolis, MN; [2]Division of Pharmaceutical Sciences, School of Pharmacy, University of Wisconsin-Madison, Madison, WI; [3]Biostatistics and Bioinformatics, Masonic Cancer Center, University of Minnesota Twin Cities, Minneapolis, MN; [4]Department of Hematology, Erasmus University Medical Center, Rotterdam, The Netherlands; [5]Cold Spring Harbor Laboratory, Cold Spring Harbor, NY; [6]Watson School of Biological Sciences, Cold Spring Harbor, NY; [7]Laboratory of Cellular Oncology, Center for Cancer Research, National Cancer Institute, Bethesda, MD; [8]Howard Hughes Medical Institute, Cold Spring Harbor, NY; [9]Comparative Pathology Shared Resource, Masonic Cancer Center, University of Minnesota Twin Cities, Minneapolis, MN; [10]Department of Laboratory Medicine, Helen Diller Family Comprehensive Cancer Center, University of California, San Francisco, San Francisco, CA; and [11]Experimental Cancer Genetics, The Wellcome Trust Sanger Institute, Hinxton, United Kingdom

Patients with a t(9;11) translocation (*MLL-AF9*) develop acute myeloid leukemia (AML), and while in mice the expression of this fusion oncogene also results in the development of myeloid leukemia, it is with long latency. To identify mutations that cooperate with *Mll-AF9*, we infected neonatal wild-type (WT) or *Mll-AF9* mice with a murine leukemia virus (MuLV). MuLV-infected *Mll-AF9* mice succumbed to disease significantly faster than controls presenting predominantly with myeloid leukemia while infected WT animals developed predominantly lymphoid leukemia. We identified 88 candidate cancer genes near common sites of proviral insertion. Analysis of transcript levels revealed significantly elevated expression of *Mn1*, and a trend toward increased expression of *Bcl11a* and *Fosb* in *Mll-AF9* murine leukemia samples with proviral insertions proximal to these genes. Accordingly, *FOSB* and *BCL11A* were also overexpressed in human AML harboring *MLL* gene translocations. *FOSB* was revealed to be essential for growth in mouse and human myeloid leukemia cells using shRNA lentiviral vectors in vitro. Importantly, *MN1* cooperated with *Mll-AF9* in leukemogenesis in an in vivo BM viral transduction and transplantation assay. Together, our data identified genes that define transcription factor networks and important genetic pathways acting during progression of leukemia induced by *MLL* fusion oncogenes. (*Blood*. 2012;119(19): 4512-4523)

Introduction

The mixed lineage leukemia or myeloid/lymphoid leukemia (*MLL*) gene found on chromosome 11q23 is involved in oncogenic translocations in adult and infant leukemia.[1] Translocations involving *MLL* are also frequently found in therapy-related leukemia when patients have received topoisomerase II inhibitors as part of their treatment.[2] *MLL* is reported to be involved in translocations with > 60 genes, all of which are thought to result in fusion proteins.[3]

The *MLL-AF9* translocation, t(9;11)(p22;q23), is the most common *MLL* translocation observed in patients with de novo and therapy-related acute myeloid leukemia (AML) and indicates an intermediate to poor prognosis with a high risk of relapse.[4,5] A knock-in mouse model for the *MLL-AF9* translocation was generated and mice heterozygous for the *Mll-AF9* knock-in allele were reported to develop AML, with 50% of the mice developing disease by 5 months of age.[6-8] However, mice presented with leukemia only after a relatively long latency, indicating that cooperating mutations are needed to contribute to leukemia progression.

Murine leukemia viruses (MuLV) have been used to identify important leukemia-associated genes in various leukemia-predisposed mutant strain backgrounds, such as *Eμ-Myc*, *Cdkn2a*$^{(-/-)}$, inversion 16, and *Nf1*$^{-/+}$ mouse models.[9-11] A recombinant MuLV that induces myeloid leukemia with a broad tropism in inbred mouse strains has been engineered by combining sequences from the amphotropic virus strain 4070A and Moloney murine leukemia virus (Mo-MuLV), designated MOL4070LTR.[12] MOL4070LTR (abbreviated here as M4070) functions as an insertional mutagen to accelerate leukemia in at least 2 mouse models of AML.[13,14] Here we use M4070 to identify mutations that collaborate with *Mll-AF9* to drive leukemogenesis in mice. To identify genes relevant to human *MLL* leukemia, a comparative oncogenomics approach with clinical patient samples was used. Functional validation of 2 genes (*FOSB* and *MN1*) support their role in leukemogenesis in concert with *Mll-AF9*.

Methods

Mice and retroviral infection

Heterozygous *Mll-AF9* C57BL/6J mice (provided by Dr Terence Rabbitts, Section of Experimental Therapeutics, Leeds Institute of Molecular Medicine) were bred to wild-type (WT) 129/SvJ mice (The Jackson Laboratory) to produce F1 offspring.[13] Two- to 4-day-old F1 offspring were inoculated intraperitoneally with 1 to 2 × 10^5 infectious particles in 0.1 mL of media. Control mice were injected with 0.1 mL of a nonviral supernatant. Four experimental cohorts were established: infected *Mll-AF9*, infected WT,

Submitted April 26, 2010; accepted March 3, 2012. Prepublished online as *Blood* First Edition paper, March 16, 2012; DOI 10.1182/blood-2010-04-281428.

The online version of this article contains a data supplement.

The publication costs of this article were defrayed in part by page charge payment. Therefore, and solely to indicate this fact, this article is hereby marked "advertisement" in accordance with 18 USC section 1734.

noninfected *Mll-AF9*, and noninfected WT. Mice were observed daily for signs of morbidity such as labored breathing, immobility, and organomegaly, at which time they were killed. Mice were housed, bred, and manipulated according to specific pathogen-free conditions set out by the University of Minnesota's Institutional Animal Care and Use Committee.

Immunophenotyping

Immunophenotyping included morphology, histopathology, flow cytometry, Southern blot, cytology, and IHC (supplemental Methods, available on the *Blood* Web site; see the Supplemental Materials link at the top of the online article).

Proviral insertion site sequencing

PCR amplification of M4070 proviral insertions was performed essentially as described previously[14] (see supplemental Methods). Splinkerette PCR products were shotgun cloned into pCR4-Topo vector (Invitrogen), transformed into electrocompetent DH10B *Escherichia coli* (ElectroMax; Invitrogen), and plated onto selective medium with ampicillin (120 μg/mL). Plasmid DNA was prepped from bacteria after 24-hour growth using alkaline lysis. Plasmid DNA was sequenced using an M13R primer and BigDye 3.1 (Invitrogen), on 3730 DNA analyzer machines (Applied Biosystems Inc).

Sequence processing and annotation

A total of 26 160 initial ABI sequence reads were processed and analyzed using a custom, semiautomated processing pipeline first described in Starr et al.[15] Nonredundant (NR) insertion positions were annotated using the EnsEMBL API[16] with the name of the gene whose start site was closest to the proviral insertion position. Common insertion site (CIS) positions were annotated similarly using the median insertion position within the CIS as a reference point (see supplemental Methods).

Quantitative real-time PCR

For quantitative real-time PCR, see supplemental Methods.

Lentiviral production and shRNA knockdown analysis

293T cells were transfected with TRIPZ lentiviral shRNAmir plasmids from Open Biosystems (Thermo Fisher Scientific) encoding shRNA to the human *FOSB* gene or a scrambled control. Lentiviral supernatant was collected after 24 and 48 hours, filtered with a 45-μm filter, and concentrated using the LentiX Concentrator (Clontech). U937 leukemia cells[17,18] were transduced with the lentivirus for 6 hours, followed by puromycin selection to produce cell lines that stably express the shRNA plasmid. To induce knockdown with the shRNA, cells were plated at 0.5 million cells per well in 6-well plates with 2 mL of media containing puromycin for 24 hours. The cells were then treated with 4 μg/μL doxycycline to induce the shRNAs.

Transduction of Tet-On MLL-AF9;Nras^{G12D} cells and shRNA induction

Experiments were performed as previously described.[19]

Western blot analysis

Cells were incubated with lysis buffer for 20 minutes on a rotator and centrifuged at 20 817*g* for 10 minutes, both at 4°. Samples were analyzed with a Bradford reaction and 40 μg of total protein were run with sample buffer on a prepared 10% Bis-Tris gel using an Invitrogen gel box at 200 V and transferred to a nitrocellulose membrane using the iBlot system (Invitrogen). Membranes were blocked with 5% nonfat milk, incubated with anti-Fosb rabbit polyclonal Ab (Cell Signaling Technology), and anti–rabbit secondary Ab (DAKO) before developing using ECL (Thermo Scientific).

BM transduction/transplantation assay

BM cells were harvested from 8- to 13-week-old *Mll-AF9*/+ and WT littermate control mice treated with 150 mg/kg 5-fluorouracil (5-FU; InvivoGen) 6 days earlier. E86 cells (stably expressing retroviruses encoding either pSF91-*MN1* or a GFP-only construct)[20] were sublethally irradiated and plated in nutrient-rich medium with a cytokine cocktail of 10 ng/mL mouse recombinant IL-6 (mIL-6), 50 ng/mL murine recombinant stem cell factor (mSCF; Invitrogen), and 5 ng/mL murine recombinant IL-3 (mIL-3; Thermo Fisher Scientific). Twenty-four hours later, the BM cells were added with 5 μg/mL polybrene (Millipore). After 48 hours, BM cells were collected and replated for expansion for 24 hours in nutrient-rich media. Recipient 8-week-old C57BL/6J.BoyJ mice were lethally irradiated at 900 rad the day before being injected intravenously with 10^6 transduced BM cells each and followed for disease progression.

Results

Infection with M4070 retrovirus accelerates leukemia development in *Mll-AF9*/+ mice

F1 animals, heterozygous for *Mll-AF9* or WT, were generated as shown (Figure 1A). Neonates were injected IP with the M4070 virus or mock infected.[21] Ninety-eight percent of the animals in both M4070-infected groups and the mock-infected *Mll-AF9* group succumbed to overt leukemia within 1 year. Infected *Mll-AF9* mice had a significantly decreased latency of disease with a median survival of 108 days compared with 165 days in noninfected *Mll-AF9* mice ($P < .0001$). Infected WT mice also developed leukemia but with a much longer latency (191 days median survival) compared with the infected *Mll-AF9* group ($P < .0001$; Figure 1B). Interestingly, *Mll-AF9* female mice died significantly faster than their male littermates, regardless of whether they were injected with the M4070 virus or not (supplemental Figure 1A-B). This finding may be related to the higher frequency of *MLL* rearrangements observed in human female infant leukemia.[22]

Virally infected *Mll-AF9*/+ mice develop predominantly myeloid leukemia

Moribund mice that died within 1 year presented with hematopoietic malignancies, often exhibiting splenomegaly, enlarged lymph nodes, thymus, and occasionally liver. Noninfected *Mll-AF9* mice showed 75% myeloid disease, characterized by a high Gr-1 and/or Mac-1 population, and 19% with distinct myeloid and lymphoid populations (MandL). The mixed myeloid and lymphoid disease in this *Mll-AF9* model is a novel discovery not described in previous reports. Phenotypic analysis revealed different lineage distribution on infection with M4070. Forty-four percent of infected *Mll-AF9* mice exhibited myeloid disease, 32% MandL, and only 17% had lymphoid disease. Conversely, the majority of the infected WT mice presented with lymphoid disease (82%), 10.3% showed myeloid disease, and only 6.4% of mice had MandL mixed disease (Figure 1C). The lymphoid populations were characterized by an extrathymic high $CD4^+$ or $CD8^+$ single-positive population, or dominant $CD4^+$ and $CD8^+$ double-positive population in the spleen or lymph nodes (supplemental Figure 3B and data not shown). This defines the first of 2 distinct classes of lymphoid disease in both virally infected groups, herein called L-1 (Figure 1C). The second class of mice were found to have T-cell lineage lymphoid disease by IHC but also expressed the Mac1 myeloid marker on the blast cell surface, herein called L-2, a phenotype not found in noninfected *Mll-AF9* animals (Figure 1C). The total

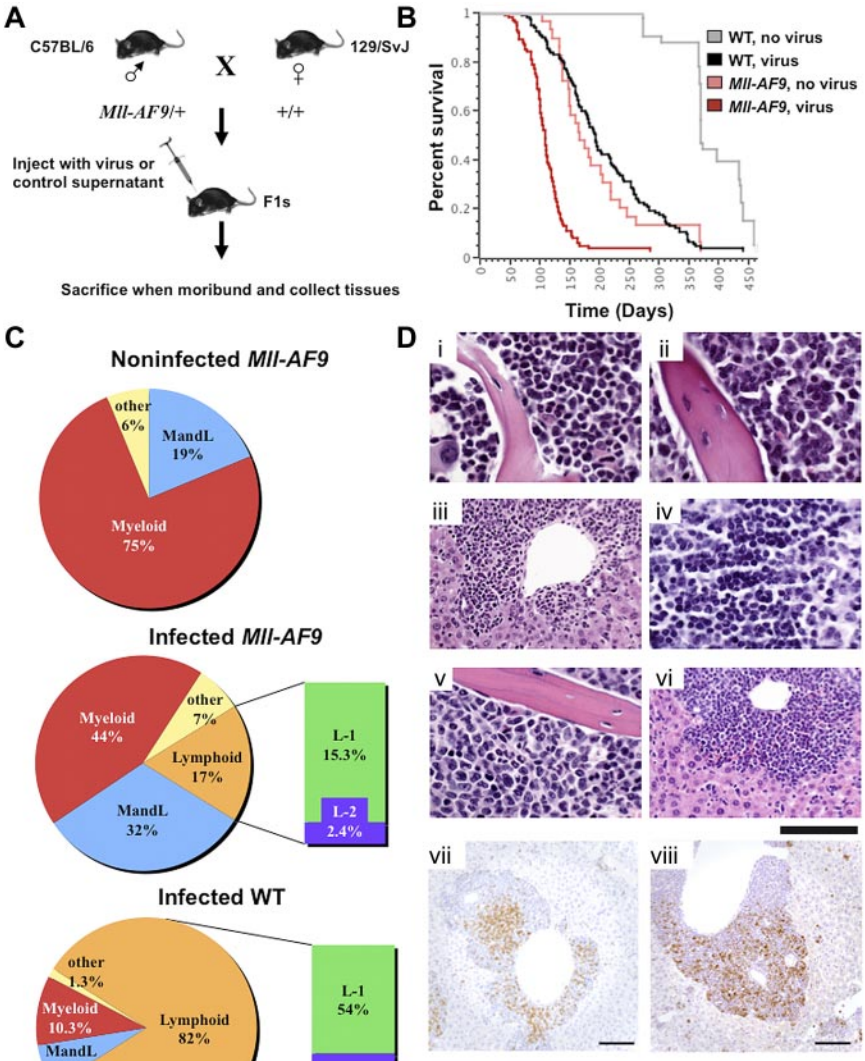

Figure 1. Insertion mutagenesis screen accelerates leukemia in experimental mice. (A) *Mll-AF9*/+ mice on a C57BL/6 genetic background were crossed to WT mice of the 129/SvJ genetic background to generate experimental cohorts. The resulting pups were infected by IP injection and followed for disease progression. Mice were killed when moribund, and tissues were collected for cloning insertions, FACS analysis, and histology. (B) Log-rank (Mantel-Cox) tests performed on a Kaplan-Meier survival plot indicate that infected *Mll-AF9* mice develop disease with a reduced latency compared with infected WT mice ($P < .0001$) and noninfected *Mll-AF9* mice ($P < .0001$). A total of 279 mice were used in the study: infected WT (n = 114), infected *Mll-AF9* (n = 97), noninfected WT (n = 40), and noninfected *Mll-AF9* (n = 28). (C) Infected WT animals develop mostly lymphoid leukemia and *Mll-AF9*/+ animals develop mostly myeloid leukemia. Pie charts depict the percentage of each leukemia type in the experimental cohorts. Myeloid disease is displayed in red, both myeloid and lymphoid disease is blue, only lymphoid disease is orange, and other diseases are yellow. Lymphoid disease is further divided into L-1 (green) and L-2 (purple). A high CD4 or CD8 population characterizes both L-1 and L-2 but L-2 also has Mac1 positively on its surface. (D) Disease phenotype in *MLL-AF9* mice infected with retrovirus. Mouse 410 showed myeloid predominance with differentiated forms in marrow (i) and spleen (not shown): myeloid neoplasm common in *Mll-AF9* mice. Mouse 529 showed immature myeloid forms in marrow (ii), infiltrate in the liver (iii), lymphoma in the thymus (iv), and a mixture of myeloid leukemia and lymphoma in the spleen (flow immunophenotype shown in supplemental Figure 3B): mixed AML and T-cell lymphoma/leukemia. Mouse 522 showed moderate myeloid differentiation in the marrow (v), infiltrate in the liver (vi), and myeloid leukemia in the spleen (flow immunophenotype shown in supplemental Figure 3C): AML. H&E. IHC of mouse 539 shows CD3 (vii) and myeloperoxidase (viii) positivity in infiltrating cells in the liver; chromogen is DAB. Scale bar represents 20 μm in subpanels i, ii, iv, and v; 50 μm in iii and vi; and 100 μm in vii and viii. Image acquisition details can be found in supplemental Methods.

number and percentage of mice with each phenotype classification from each experimental cohort is shown in supplemental Figure 2A.

A common method to determine lineage is to assess TCR or BCR rearrangements. However, when we examined leukemias in all 3 cohorts (infected *Mll-AF9*, noninfected *Mll-AF9*, infected WT) for clonal Jβ1 or Jβ2 (T-cell) or JH (B-cell) receptor gene rearrangements, we frequently saw evidence of TCR and/or BCR rearrangements even if they were phenotypically determined to be myeloid disease. In fact, most *Mll-AF9* mice had myeloid disease but almost 50% of myeloid tumors were positive for clonal TCR or BCR rearrangements. Moreover, 20% of animals with lymphoid disease were negative for clonal T- or B-cell rearrangements (supplemental Figure 2B). Thus, the presence or absence of a TCR and/or BCR rearrangement is neither completely sensitive nor specific to a lymphoid phenotype, and is on its own insufficient to assess lineage. To determine which phenotype qualifiers were statistically significantly associated, Fisher exact tests were performed on each pairwise comparison of the total phenotype condition and each phenotype variable (supplemental Table 1A). A myeloid or MandL phenotype was positively correlated with a larger spleen weight, the *Mll-AF9*/+ genotype, and only in the case of myeloid disease, an extremely elevated white blood cell (WBC) count whereas there were multiple reciprocal positive correlations between lymphoid phenotypes, BCR and/or TCR rearrangements, a normal spleen weight, and WT leukemias.

Pathologic analyses illustrated the disruption of normal tissue architecture by tissue infiltration of leukemic blast cells in virally infected *Mll-AF9* mice (Figure 1D). *Mll-AF9* mice, both infected and noninfected, commonly showed a differentiated myeloid neoplasm in the marrow (Figure 1Di). A subset of both infected *Mll-AF9* and infected WT mice presented with mixed myeloid leukemia and T-cell lymphoma/leukemia in the liver, marrow, thymus, and spleen of the animal, with CD3 and myeloperoxidase-positive cells detectable in infiltrating cells by IHC (Figure 1Dii-iv,vii-viii). There were also *Mll-AF9* mice that exhibited classic AML in the marrow and liver (Figure 1Dv-vi). Cytology was also performed to confirm the maturity and cell type of the disease in infected *MLL-AF9* mice. Examples are shown in supplemental Figure 3A which includes cytology of a well-differentiated myeloid leukemia, a blastic myeloid leukemia, a lymphoid leukemia/lymphoma, and a moderately differentiated myeloid leukemia. Supplemental Figure 3B depicts flow cytometry data from a representative mouse with 2 different diseases (mixed AML and T-cell lymphoma/leukemia) as was observed in both

infected WT and infected *Mll-AF9* cohorts. Its corresponding pathology is shown in Figure 1Dii-iv. The myeloid immunophenotype characteristic of the *Mll-AF9* mice is shown in supplemental Figure 3C, whose corresponding pathology is in Figure 1Di.

Survival curves were generated to determine whether the reduced latency in M4070-infected *Mll-AF9* mice was associated with a particular phenotype. The survival of *Mll-AF9* mice was significantly decreased compared with WT mice regardless of phenotypic class (supplemental Figure 1C-E). Importantly, the disease latency did not show dependence on phenotype within the WT or *Mll-AF9* groups of mice (supplemental Figure 1F-H). Thus, the genetic mutations induced by the M4070 virus influenced leukemia progression as governed by the initiating mutation. Therefore, infection accelerated mostly myeloid leukemia *Mll-AF9*/+ mice, while causing mostly lymphoid leukemia in WT mice.

Cloning retroviral integrations leads to identification of CISs

Ligation-mediated PCR was used to amplify the M4070-genomic DNA junctions in 165 independent M4070-infected leukemia samples (both *Mll-AF9* and WT). A total of 1745 nonredundant insertions or unique reference sequences, representing an average of 10.8 insertions per tumor, were recovered. Sequences are available through the public mouse Retroviral Tagged Cancer Gene Database (RTCGD).[23] In total, 88 unique CISs were identified by established statistical analysis and the additional criterion that proviral insertions in leukemia samples must come from at least 3 mice (see supplemental Methods and Table 1). Sixty-nine CISs were recovered by combining all insertions from both infected *Mll-AF9* leukemia and infected WT leukemia. Additional CISs came from analysis of only insertions in *Mll-AF9* leukemia (15) and infected WT leukemia (4). The rest of the CISs from the WT leukemia group (supplemental Table 2) and *Mll-AF9* leukemia group (supplemental Table 3) overlapped with the combined dataset. Southern blotting using an M4070-specific probe showed that the proviral insertions in infected animals were clonal to oligoclonal with one internal proviral fragment represented by a band common to all tumors and additional unique M4070 insertions (supplemental Figure 4). No proviral insertions were detected in noninfected animals, and M4070 insertions were consistent throughout each diseased animal (data not shown).

The CISs were distributed throughout the mouse genome (Figure 2A). Examples of 2 CIS regions and the proviral insertions that define them are displayed in Figure 2B and C. We defined a CIS-associated gene as the gene with the transcription start site closest to the median of the CIS region, which became a candidate gene for a role in leukemia progression.

Twenty-nine candidate genes, of the 88 CIS-associated genes identified, have been previously identified in other genetic screens according to the RTCGD.[23] Sixty-nine of the human homologs of candidate genes are mutated in human cancer according to the Catalog of Somatic Mutations In Cancer (COSMIC),[24] and 13 are known cancer genes according to the Cancer Gene Census,[25] including genes associated with leukemia such as *Cyclin D1, Fgfr3, Myc*, *Ikaros, Notch1, Myb, Bcl11a,* and *Mn1* (Table 1). Ingenuity pathway analysis shows that our candidate gene list falls into 3 main functional categories: cell transformation, blood cell development, and cell differentiation (supplemental Table 4A). In addition, the top 5 overrepresented canonical pathways from this list of candidate genes are linked to acute and chronic myeloid leukemia genes (supplemental Table 4B).

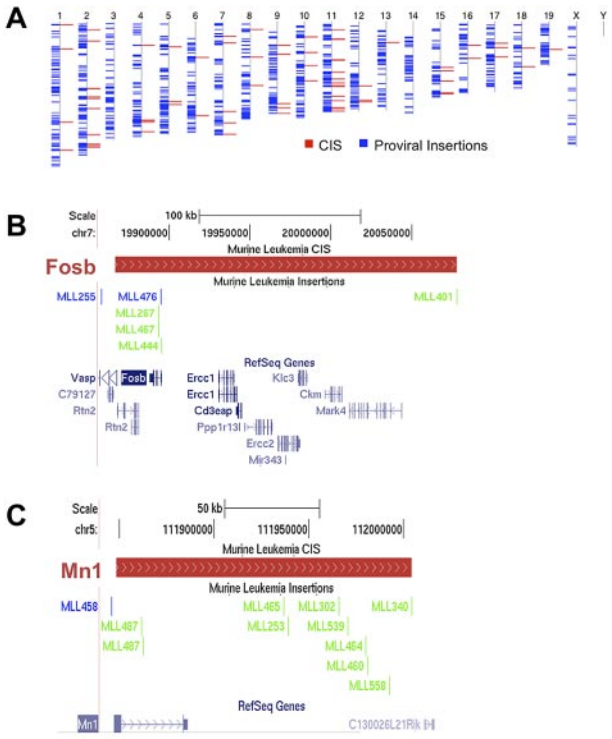

Figure 2. Proviral insertions are randomly distributed throughout the genome and define CISs. (A) Blue lines represent all the insertions recovered from the screen overlaid on the mouse chromosomes, labeled above. Red lines represent all the resulting CISs. (B-C) Two representative CISs with the distribution of insertions. (B) Insertions defining *Fosb*; (C) insertions defining *Mn1*. The red bars define a CIS region. The scale and chromosome region are above the CIS region while the insertions from the different mice in the screen are below. With respect to the primary CIS-associated genes, blue lines on the insertion track indicate positive orientation and green lines indicate a negative orientation. RefSeq genes within the CIS are in blue at the bottom of each figure.

Analysis of candidate leukemia genes leads to identification of *Mn1*, *Fosb,* and *Bcl11a* as candidate *MLL-AF9* cooperating genes

To prioritize genes that may cooperate with *Mll-AF9* to cause leukemia progression from the 88 candidate genes as listed in Table 1, we determined the percentage of leukemias containing an insertion within each independent gene for each of the 3 analysis groups (WT, *Mll-AF9*, and combined). The candidate genes were sorted in alphabetical order and visualized in a heat map (Figure 3). We labeled genes as low priority if they had frequent insertions in all 3 groups, such as 3 of the 4 most frequently mutated genes (*Gfi1, Myc,* and *Myb*), or those only found in a high percentage of leukemia in the WT CIS list but not the *Mll-AF9* CIS list, such as *Hhex*, *Ikaros (Ikzf1*), and *Notch1,* a CIS without a single insertion in *Mll-AF9* mice. We then selected genes as a top priority those found in a high percentage of mice in the *Mll-AF9* CIS list but not the WT CIS list include *Bcl11a, Fosb, Mn1*, and a *Gimap* gene cluster.

Fisher exact tests were performed on each pairwise comparison of the genotype, phenotype, and CIS-associated gene. A modified heat map shows the statistically significant pairs in each genotype. The lymphoid phenotypes (lymphoid, L1 and L2) were enriched in the WT leukemia as well as 5 CIS-associated candidate genes, including *Notch1* and *Ikaros* (Figure 4A). Conversely, the *Mll-AF9* mice showed enrichment in the myeloid and MandL phenotype groups as well as 3 candidate genes, including *Mn1* and *Fosb* genes (Figure 4B). The significant associations between phenotypes,

Table 1. CIS list

Chromosome	CIS position	CIS range, kb	*Mll-AF9* mice with insert	WT mice with insert	RTCGD	Cancer Gene Census	COSMIC	All genes in/near CIS
1	4485458-4486321	1	2	1			YES	*Sox17**
1	36823950-37002868	179	3	1			YES	*Tmem131,* Zap70, AC123854.2*
1	135756752-135974231	217	2	2				*AC157924.6,* Prelp, Fmod, Btg2, Optc*
1	173849175-174012079	163	4	1	YES		YES	*Slamf6,* Copa, Vangl2, Nhlh1, AC158930.1, Ncstn*
2	11547443-11577841	30	3	0	YES		YES	*Il2ra**
2	26315310-26525572	210	0	11	YES	YES	YES	*Notch1,* mmu-mir-126, Egfl7, Agpat2, Fam69b, AL732311*
2	90344091-90491625	148	3	1			YES	*Ptprj**
2	90919486-90925879	6	3	1			YES	*Slc39a13,* Sfpi1*
2	101463219-101464091	1	4	0				*B230118H07Rik,* Rag2*
2	103601727-103784302	183	1	3	YES	YES	YES	*Lmo2,* Nat10, Caprin1, BX537331.1, AL928544.7 (miRNA), AL928544.5 (miRNA)*
2	103601727-103784302	183	0	3			YES	*Nat10,*† Lmo2, Caprin1, BX537331.1, AL928544.7 (miRNA), AL928544.5 (miRNA)*
2	117168903-117367506	199	3	10	YES		YES	*Rasgrp1**
2	152601718-152828604	227	2	2	YES		YES	*Bcl2l1,* Tpx2, Mylk2, Ttll9, Foxs1, Dusp15*
2	165712889-165837434	125	4	0				*Prkcbp1,* Zmynd8, Ncoa3*
2	165781678-165837434	56	3	0				*RP23-108D12.5*‡*
2	167625651-167785437	160	4	1				*A530013C23Rik,* Ptpn1*
2	167750534-167785437	35	3	0			YES	*Ptpn1*‡*
2	169958430-170046828	88	2	2	YES		YES	*Zfp217**
3	94945270-95035953	91	3	0			YES	*Tnfaip8l2,*‡ Cdc42se1, Sema6c, Gabpb2, Mlt11, Gm128, Bnipl, Lysmd1, Scnm1*
4	32341351-32513306	172	3	3	YES		YES	*Bach2**
4	133220770-133371434	151	2	2			YES	*Pigv,* Aridla*
4	133652224-133867470	215	1	2	YES		YES	*Cd52,* Ubxn11, Aim1, Sh3bgrl3, Ccdc21, Gm7534, Catsper4, Cnksr1, Zfp593, Grrp1, Pdik1*
4	149076009-149079348	3	2	1			YES	*Pik3cd**
5	34038901-34279652	241	1	3	YES	YES	YES	*Fgfr3,* Tacc3*
5	108078270-108186428	108	5	19	YES		YES	*Gfi1,* Evi5, Rpap2*
5	111845647-112004142	158	10	3	YES	YES	YES	*Mn1,* C130026L21Rik*
6	48598556-48720382	122	6	0			YES	*Gimap8,* Gimap cluster*
6	48630644-48720382	90	5	0			YES	*Gimap4,*‡ Gimap* cluster
6	127104034-127281434	177	2	5	YES	YES	YES	*Ccnd2,* AC161597.1*
7	19858212-20077994	220	6	0			YES	*Fosb,* mmu-mir-343, Ercc1, Ercc2, Ppplrl3, Rtn2, Ckm, Exoc3l2, C79127, Vasp, Cd3eap, Klc3, Mark4*
7	29165895-29228553	63	4	0			YES	*Gmfg,* Paf1, Samd4b, Med29*
7	121285480-121354575	69	5	11	YES		YES	*Rras2,* Copb1*
7	136903269-136957718	54	2	2	YES			*Brwd2**
7	152126941-152233702	107	3	2	YES	YES	YES	*Ccnd1,* Oraov1*
8	10856578-11099413	243	3	3				*AC116499.9,* 3930402G23Rik, Irs2*
8	10910498-11099413	189	0	3	YES			*3930402G23Rik,*† Irs2*
8	86266601-86296089	29	2	1			YES	*Cd97**
8	131049443-131116479	67	3	0			YES	*Nrp1*‡*
9	32416427-32624588	208	3	5	YES		YES	*Ets1**
9	44135577-44376194	241	2	1			YES	*Dpagt1,* Bcl9l, H2afx, Hyou1, Rps25, Slc37a4, AC122428.3, C030014l23Rik, C2cd2l, Hmbs, Vps11, Trappc4, Ccdc84, Foxr1, Upk2, AC122428.2, Cxcr5*
9	110800877-110812241	11	2	1			YES	*Als2cl**
9	123758644-123985636	227	3	1			YES	*Fyco1,* Xcrl, CAAA01140679.1.6228.1, Ccr1, Ccr1l1, Ccr3*

List of all CISs from insertion site analysis. Columns 1 and 2 are the chromosome and position of each CIS according to NCBI build 37. Column 3 shows the range of the CIS in kilobases. Columns 4 and 5 are the number of each genotype with contributing insertions to each CIS. Columns 6 to 8 refer to the gene shown with an asterisk in column 9. Column 6 indicates whether the gene has previously been identified in the RTCGD,[23] column 7 indicates whether the human homolog of the gene has been identified as a cancer gene in the Cancer Gene Census,[25] and column 8 indicates whether a mutation in the human homolog of the gene has been identified as a recurring somatic mutation in cancer (COSMIC).[24] Column 9 shows all the genes in or near the CIS region that may be affected by proviral insertions.

CIS indicates common insertion site; RTCGD, Retroviral Tagged Cancer Gene Database; COSMIC, Catalog of Somatic Mutations In Cancer; and WT, wild type.

*The gene whose transcriptional start site is closest to the median of the CIS region, which was called the CIS-associated candidate gene, annotated using Ensembl release 55.

†Genes are only found in the infected WT CIS analysis.

‡Genes are found only when analyzing CIS from infected *Mll-AF9* mice.

Table 1. CIS list (continued)

Chromosome	CIS position	CIS range, kb	*Mll-AF9* mice with insert	WT mice with insert	RTCGD	Cancer Gene Census	COSMIC	All genes in/near CIS
10	20763054-20972634	210	8	9	YES	YES	YES	*Myb,* Ahi1, AC153556.5 (miRNA)*
10	20811983-20972634	161	0	9				*AC153556.5,*† Myb*
10	41658107-41790233	132	1	3			YES	*Armc2**
10	59615644-59634420	19	2	1			YES	*Chst3,* Spock2*
10	76990210-77085753	96	3	0			YES	*Itgb2,*‡ 181008A18Rik, Pttglip, Sumo3, Ube2g2*
10	79452089-79621648	170	4	0			YES	*Cnn2,* Abca7, Hmha1, Gpx4, Stk11, Atp5d, Midn, ORF61, Polr2e, Sbno2, Dos*
10	79895567-80140544	245	2	2			YES	*Mknk2,* Tcf3, Onecut3, Atp8b3, Rexo1, Klf16, Fam108a, Scamp4, Adat3, Csnk1g2, Btbd2*
10	92532859-92627678	95	3	0				*4930485B16Rik,*‡ Cdk17*
11	11465042-11679166	214	2	8	YES	YES	YES	*Ikzf1,* 4930512M02Rik, AL596450.1, RP23-373H2*
11	23642090-23679371	37	2	1	YES	YES	YES	*Rel**
11	24098976-24156602	58	6	2	YES	YES	YES	*Bcl11a**
11	51713117-51817285	104	4	0			YES	*Phf15,* Cdkn2aipn1, Ube2b, Cdkl3*
11	52118189-52155248	37	2	2			YES	*Tcf7,* Vdac1*
11	68174513-68271352	97	1	4	YES		YES	*Pik3r5,* Ntn1, AL606831.2 miRNA*
11	77601654-77615704	14	2	1			YES	*Myo18a,* AL591065.2*
11	79467420-79566569	99	3	0			YES	*Rab11fip4,*‡ mmu-mir-193 (miRNA), mmu-mir-365-2 (miRNA), AL731726.1*
11	86407328-86438598	31	3	0				*Tmem49**
11	87565872-87567954	2	2	1	YES			*mmu-mir-142**
11	100752419-100753004	1	2	1			YES	*Stat3**
11	106548821-106782459	234	2	3				*Gm885,* Pecam1, Polg2, AL593847.1, Smurf2, Ddx5, Ccdc45*
11	115872987-116120321	247	2	3			YES	*Galk1,* Trim65, Srp68, Itgb4, H3f3b, Unk, Uncl3d, Trim47, Mrpl38, Wbp2, Fbf1, Acox1, Evpl, Cdk3, 2310004N24Rik*
11	117205625-117212544	7	2	1	YES		YES	*Sept9**
11	120491729-120493009	1	3	0			YES	*Mafg**
12	86976896-87168328	191	2	2			YES	*Jdp2,* Ttll5, 0610007P14Rik, Batf, Mfsd7c*
12	108362175-108363890	2	1	2				AC163345.1*
13	28644507-28873369	229	3	2				*RP23-45H23.1,* Sox4, RP23-371K8*
14	70133928-70229580	96	3	0			YES	*Chmp7,*‡ Tnfrsf10b, Rhobtb2, Pebp4*
15	61815622-62044652	229	6	9	YES	YES	YES	*Myc,* Pvt1*
15	62000405-62022073	22	3	0				*Pvt1*‡*
15	66633426-66693812	60	3	1			YES	*Sla,* Tg*
15	66646986-66693812	47	3	0			YES	*Tg,*‡ Sla*
15	80346987-80525653	179	4	2			YES	*Enthd1,* Grap2, Fam83f*
15	96373651-96486074	112	3	0				*AC123606.11,*‡ Slc38a1, Slc38a2*
15	96373651-96540760	167	3	2	YES		YES	*Slc38a1,* Slc38a2, AC123606.1*
15	97443447-97669490	226	4	0			YES	*Rpap3,* Pp11r, Hdac7, Rapgef3, AC104225.2, Slc48a1, Vdr*
16	32433625-32549358	116	3	1				*Pcyt1a,* Zdhhc19, Osta, Tctex1d2*
16	32517604-32549358	32	3	0			YES	*Zdhhc19*‡*
16	49771352-49938369	167	4	0			YES	*Ift57,* Cd47G, m5486, AC107830.1, AC107830.2*
16	49839166-49938369	99	3	0			YES	*Cd47*‡*
17	29534871-29639166	104	6	7	YES	YES	YES	*Pim1,* Fgd2*
17	47649930-47875555	226	1	4			YES	*Taf8,* Tcfeb, Med20, Frs3, Pgc, Usp49, Ccnd3, Bysl, Tomm6, Prickle4*
17	52420984-52490384	69	3	0				*AC121600.2,*‡ AC121600.1 (miRNA)*
18	35900301-36089864	190	2	3			YES	*Tmem173,* Cxxc5*
18	60962858-60989942	27	2	1		YES	YES	*Cd74,* Tcof1*
19	37514331-37569767	55	4	6			YES	*Exoc6,* Hhex*
19	37514331-37569373	55	0	6	YES		YES	*Hhex,*† Exoc6*

List of all CISs from insertion site analysis. Columns 1 and 2 are the chromosome and position of each CIS according to NCBI build 37. Column 3 shows the range of the CIS in kilobases. Columns 4 and 5 are the number of each genotype with contributing insertions to each CIS. Columns 6 to 8 refer to the gene shown with an asterisk in column 9. Column 6 indicates whether the gene has previously been identified in the RTCGD,[23] column 7 indicates whether the human homolog of the gene has been identified as a cancer gene in the Cancer Gene Census,[25] and column 8 indicates whether a mutation in the human homolog of the gene has been identified as a recurring somatic mutation in cancer (COSMIC).[24] Column 9 shows all the genes in or near the CIS region that may be affected by proviral insertions.

CIS indicates common insertion site; RTCGD, Retroviral Tagged Cancer Gene Database; COSMIC, Catalog of Somatic Mutations In Cancer; and WT, wild type.

*The gene whose transcriptional start site is closest to the median of the CIS region, which was called the CIS-associated candidate gene, annotated using Ensembl release 55.

†Genes are only found in the infected WT CIS analysis.

‡Genes are found only when analyzing CIS from infected *Mll-AF9* mice.

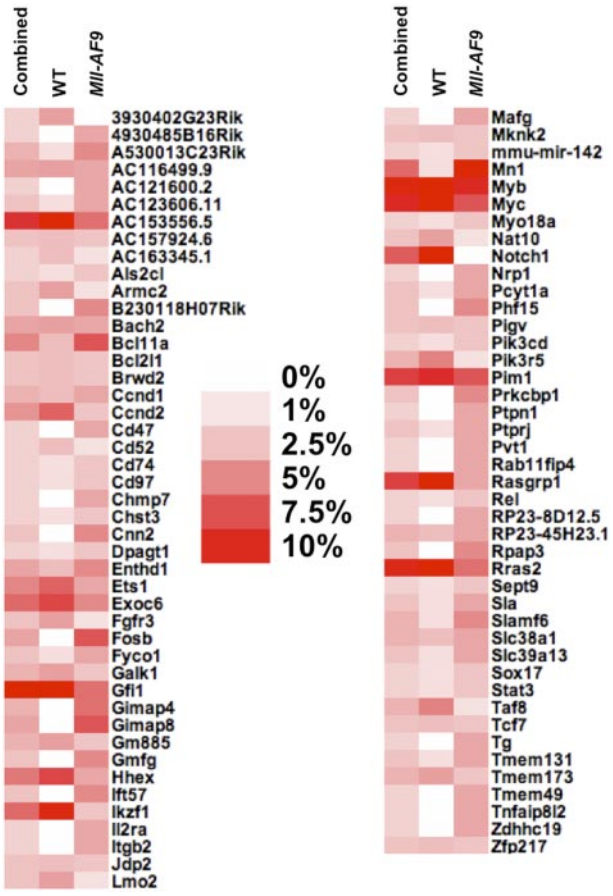

Figure 3. Heat map shows the percentage of mice containing an insertion in each CIS of the total number of mice with at least one insertion. Combined, WT, and *Mll-AF9* refer to the 3 different CIS analyses that were performed, where combined means all insertions from both genotypes were used. The darkest red color indicates that more than 10% of the mice in that CIS list have insertions in a given CIS-associated gene, while white indicates no mice had insertions near a given gene in that CIS list, as indicated in the legend.

genotypes, and genes are displayed in a network where each line represents a significant pairwise connection that allows visualization of all the associations simultaneously (Figure 4C). The significant associations between phenotype variables and specific candidate genes are listed in supplemental Table 1B. Several genes associated with myeloid disease or *Mll-AF9* mice (*Gmfg, Bcl11a, Mn1*) were positively associated with a high spleen weight or high WBC count. As expected, several genes already shown to be associated with the WT genotype and lymphoid disease such as *Rasgrp1*, *Rras2*, and *Notch1* were also associated with Jβ1 or Jβ2 rearrangement. Fisher exact tests were also performed between each candidate gene pair to determine whether 2 genes occurred more frequently together than would be expected by chance. These connections are also included in the enrichment network (Figure 4C). Taken together, these data led us to pursue *Mn1, Fosb,* and *Bcl11a* for further study as potential *MLL-AF9* cooperating genes.

Candidate leukemia genes have aberrant expression in human leukemia

To determine the relevance of the genes detected in this screen in human leukemia, we compared our CIS-associated candidate genes with published data on gene expression and copy number in human leukemia samples. First, we used gene expression profile (GEP) analysis performed on data from a cohort of 461 patients with AML[26,27] to look for expression of the human homologs of our top 3 candidate *MLL-AF9* cooperating genes: *FOSB, MN1,* and *BCL11A*. We found expression of all 3 genes in AML patients at varying levels, illustrating the heterogeneity of gene expression in human AML (supplemental Figure 5A). *MN1* expression was low overall in human AML but higher on average in 2 AML subsets: patients with 3q rearrangements and inversion 16 patients. The inversion 16 observation is consistent with a previous publication.[28] Expression of *FOSB* was detected in ~ 50% of AML patients analyzed with either *MLL-AF9* translocations or with other 11q23 translocations. *BCL11A* was also expressed in all *MLL* rearranged AMLs at varying levels (supplemental Figure 5B).

We then analyzed expression in a subset of the primary AMLs with *MLL* rearrangements.[27] No significant differences in mean expression for *FOSB* and *BCL11A* were observed in patients with *MLL-AF9* AMLs or other *MLL* rearrangements compared with normal total BM (TBM) and $CD34^+$ cells (Figure 5A). However, in the case of each gene, some leukemia samples had higher expression than the highest expressing TBM and/or $CD34^+$ samples. These data suggest a possible role for *FOSB* and *BCL11A* as *MLL-AF9*–cooperating genes.

In addition, we looked for recurrent changes in gene copy number in human AML and acute lymphoblastic leukemia (ALL) of other genes from this screen. Regions of chromosome gain and loss in pediatric ALL samples from St Jude's Children's Hospital[29] were compared with the map positions of the human homologs of all CIS-associated candidate genes. Surprisingly, we found that eleven of our candidate genes overlap with 8 different areas of chromosomal deletion (Figure 5B), suggesting some pathways may be deregulated in lymphoid leukemia at least in part by deletion. There were also 2 regions of chromosomal gain that overlapped with 2 of our candidate leukemia genes (Figure 5C). One is a novel gene (*AC157924.6*) and the other is *MYB*, the amplification of which has been implicated in lymphoid and myeloid leukemia development.[30,31] Similarly, one CIS overlapped with a region of chromosomal gain containing *MYB* when using data from human AML samples collected at Washington University in St Louis.[32] However, minimal recurring copy number alterations were found in human AML overall, suggesting other mechanisms may lead to aberrant AML gene expression, such as epigenetic modifications.

Candidate *MLL-AF9* cooperating genes have aberrant expression in mouse myeloid leukemia samples

To confirm that proviral insertions affect expression of CIS-associated candidate genes in leukemia samples with insertions near those genes, we compared expression to leukemia samples that do not contain proviral insertions near these genes. Intron-spanning primers were designed for 15 candidate genes, and quantitative real-time PCR (qRT-PCR) was performed on RNA isolated from leukemias and from the corresponding tissue (lymph nodes, thymus, or spleen) from normal WT animals as baseline. Notably, *Mn1* expression was significantly increased in *Mll-AF9* myeloid leukemia tissues with insertions near *Mn1* compared with *Mll-AF9* myeloid leukemia tissues without insertions near *Mn1* ($P < .05$; Figure 6A). In this case, we found that distal insertions 100 kb downstream of *Mn1*, but near a novel gene called *C130026L21Rik,* also affected *Mn1* expression. A trend toward increased expression in myeloid leukemia from mice with insertions near *Fosb* and *Bcl11a* was also observed (Figure 6B-C). We found that *Rras2* ($P < .05$) and *Notch1* ($P < .05$) expression was significantly increased in infected WT leukemic tissues with insertions near those specific genes compared with infected WT

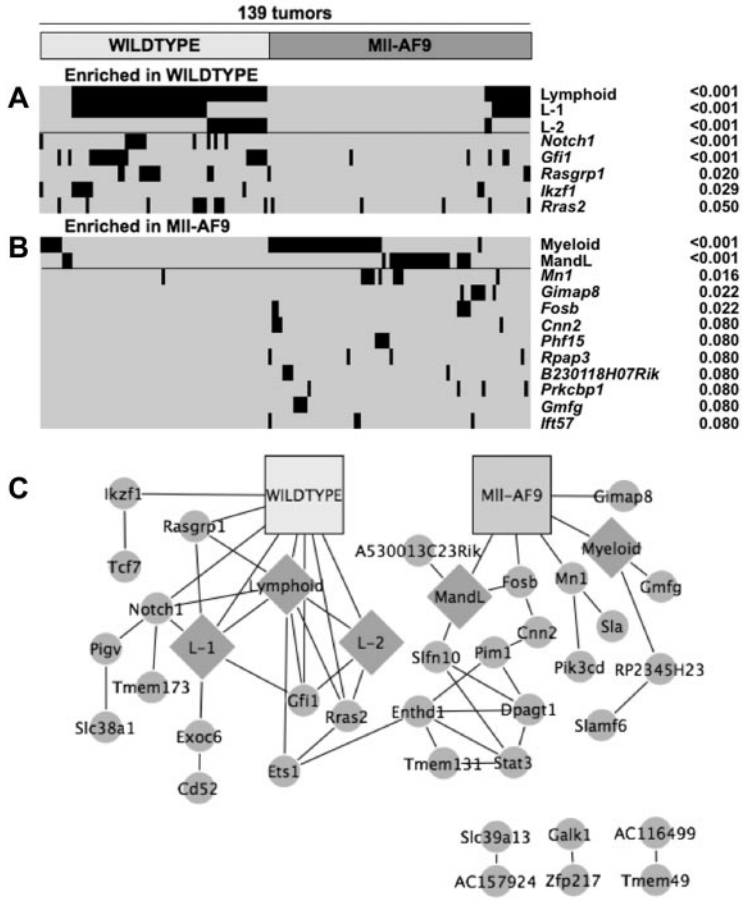

Figure 4. There are significant associations between CIS-associated candidate genes and disease phenotypes, experimental cohorts, and other CIS-associated candidate genes. Modified heat map of significant candidate gene and phenotype enrichment in (A) WT and (B) *Mll-AF9* mice. Each horizontal tick mark represents a proviral insertion identifying a CIS or a positive marker for a given phenotype in a given mouse leukemia. Mice are divided into the 2 infected genotypes across the x-axis; significant phenotypes and candidate genes are along the y-axis. Positive significant associations of phenotypes and candidate genes are shown ($P < .05$). In addition, candidate genes are shown that were found in 4 separate animals only in *Mll-AF9* leukemias ($P = .08$). (C) Network of significant associations between phenotypes, genotypes, and candidate genes. All associations with P values $< .05$ were used. Genotypes are shown in squares, phenotypes are shown in diamonds, and CIS-associated candidate genes are shown in circles.

leukemic tissues without insertions near those genes (data not shown).

Functional validation of candidate genes cooperating with *MLL-AF9* in AML leukemogenesis

To validate the importance of *FOSB* in *MLL-AF9* leukemia, we down-regulated expression using shRNA in leukemic cell lines. Human myeloid cell lines stably expressing doxycycline inducible shRNA versus *FOSB* were created. The U937 cell line, which has a *CALM-AF10* translocation and up-regulation of *HOXA9* and *MEIS1*,[33] similar to *MLL-AF9* fusion leukemias,[34] was used as a surrogate line. U937 cells expressing shRNA constructs against *FOSB* or a scrambled shRNA were induced with doxycycline or treated with vehicle for 4 days. The cell lines without induction of shRNA or with the scrambled construct showed normal proliferation in exponential growth phase while the 2 cell lines expressing shRNA against *FOSB* had significantly impaired growth over 5 days (Figure 7A). In addition, we transduced Tet-On-competent MLL-AF9;Nras^{G12D} murine cells[19] with TRMPV-Neo-shRNA constructs targeting *Fosb* or *Renilla* luciferase as a control. After doxycycline treatment, 2 *Fosb*-specific shRNAs (FosB.1165 and FosB.436) depleted shRNA-expressing AML cells (Figure 7B). Western blot analysis was used to confirm knockdown for both experiments (supplemental Figure 7). This shows that continued expression of *FOSB* is required for leukemia maintenance of 2 AML cell lines, one expressing the MLL-AF9 fusion oncogene.

It has been previously reported that knockdown of *MN1* in 2 human AML cell lines with *MLL-AF9* impairs growth.[35] To determine whether *MN1* can cooperate with *MLL-AF9* in vivo, retroviral BM transduction/transplantation assays were performed. BM from 5-FU–treated *Mll-AF9* or WT mice was harvested, transduced with a retrovirus encoding a candidate gene (pSF91-*MN1*[20]) or a GFP-only construct, and transplanted back into 129/BL6 F1 syngeneic recipient mice. Mice that received *Mll-AF9* BM transduced with the *MN1* gene succumbed to disease significantly faster with a median survival of 43 days compared with 52 days in mice transplanted with WT BM expressing *MN1* ($P = .0046$) or 136 days in mice transplanted with GFP-transduced *Mll-AF9* BM ($P < .0001$; Figure 7C). The GFP vector DNA was detected in all animals, verifying the viral transduction was successful (data not shown). The majority (25 of 27) of the animals from the 3 experimental groups with *MN1* and/or *Mll-AF9* had histopathology consistent with myeloid leukemia (data not shown). Thus, these data show *MN1* can cooperate with *MLL-AF9* in the induction of myeloid leukemia in vivo, strongly supporting a role for MN1 in myeloid transformation in MLL leukemia.

Discussion

Here, we report the findings of a large-scale MuLV insertional mutagenesis screen in an *MLL* translocation mouse model. We show that the M4070 chimeric retrovirus can accelerate myeloid and lymphoid disease in *Mll-AF9* knock-in mice and can cause lymphoid disease in WT mice. MuLV retroviral insertions in leukemias identified 88 CISs, and the enrichment of insertion mutations in some CIS-associated candidate genes in *Mll-AF9* leukemias suggested that they might cooperate with *Mll-AF9* in the

A

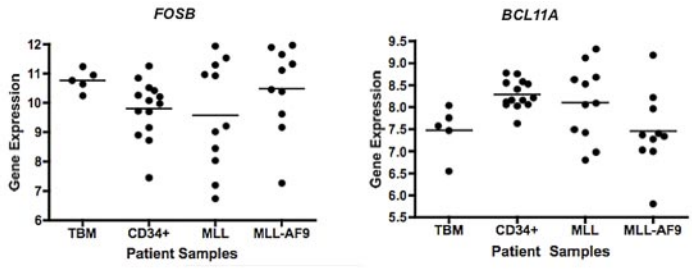

B

Murine orthologous regions of human ALL chromosomal loss			
Mouse Chr	start	end	CIS in region
2	101457598	101466316	**B230118H07Rik**
2	103638585	103783499	**Lmo2**
4	114721100	152747084	**Pik3cd, Pnrc2, Cd52, Pigv**
6	124254463	128390200	**Ccnd2**
9	44225134	44626936	**Dpagt1**
10	41609665	41679151	**Armc2**
10	78989697	79856036	**Mknk2**
11	62588426	74416023	**Pik3r5**

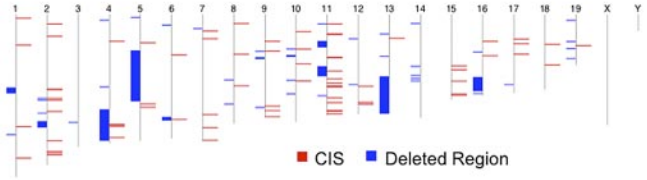

C

Murine Orthologous regions of human ALL Chromosomal Gain			
Mouse Chr	start	end	CIS in region
1	132334680	171523483	**AC157924.6**
10	20766710	20869281	**Myb***

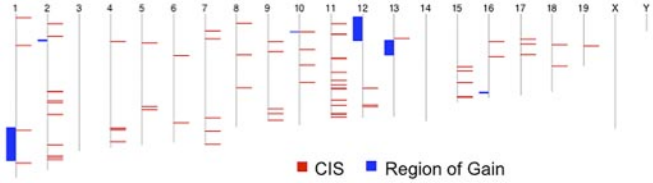

Figure 5. Human GEP and gene copy number data for candidate *Mll-AF9* cooperating genes. (A) Dot plots of expression of 2 CIS-associated candidate gene homologs in AML patients: *FOSB* and *BCL11A*. A representative probe for *BCL11A* is shown. Total BM (TBM) and CD34$^+$ cells from healthy patients (n = 5 and 14, respectively) were used as controls compared with AMLs with any *MLL* rearrangement (n = 11), and patients with *MLL-AF9* translocations (n = 10). The horizontal line represents the mean for each patient sample group. Data were log2 transformed. (B) Murine genomic regions orthologous to regions of deletion in human patients with ALL. In the bottom panel, the human chromosome map is shown. Blue blocks represent regions of chromosome deletion in ALL patients, and red blocks represent the combined CISs from our murine screen. Genes annotated using Ensembl release 55. (C) Murine genomic regions orthologous to regions of duplication or gain in human patients with ALL. In the bottom panel, the human chromosome map is shown. Blue blocks represent regions of chromosome gain in ALL patients, and red blocks represent the combined CISs from our murine screen. Genes annotated using Ensembl release 55. *Gene in region of gain in human AML that overlapped with a CIS from our murine screen.[32]

development of leukemia. Human microarray expression data were examined for the altered expression of candidate genes and showed a subset of *MLL* translocation-positive and *MLL-AF9* AMLs had higher levels of these candidate genes than controls. There was aberrant expression of candidate *Mll-AF9* cooperating genes *Mn1*, *Bcl11a*, and *Fosb* in murine leukemia samples by qRT-PCR. Finally, *FOSB* was shown to be essential to leukemia maintenance by in vitro shRNA knockdown and cooperation of *MN1* with *Mll-AF9* was confirmed with in vivo transduction/transplantation studies.

The M4070-infected WT mice developed mostly T-cell ALL whereas the M4070-infected *Mll-AF9* transgenic mice mostly developed myeloid leukemia. Moreover, the latency of disease was significantly reduced for infected *Mll-AF9* mice compared with infected WT mice (Figure 1B), suggesting that the mutations induced by M4070 cooperated with the *Mll-AF9* allele in these mice. The differences in phenotype may be caused by differences in target cell availability in the 2 groups as *Mll-AF9* mice have myeloproliferation before development of leukemia.[7] Interestingly, approximately one-third of the animals in the infected *Mll-AF9* group and 6% percent of the infected WT mice exhibited disease consisting of myeloid and lymphoid lineages. Thus, M4070 seems to accelerate ALL as well as AML, even in the same animal. It also appears fewer mutations are needed for transformation to overt leukemia in the presence of *Mll-AF9* because of its potent oncogenic quality. WT leukemias contain on average more highly penetrant CISs (CISs with insertions from at least 5 leukemias; 2.13) than *Mll-AF9* leukemias (1.43; supplemental Figure 6).

One of the goals of this article was to accurately define the phenotype of each mouse by collecting extensive complementary data using several established methods. For example, TCR and BCR gene rearrangement status has often been used to diagnose lymphoid leukemia without other data. Here, we show that this approach may be inadequate and that other methods must also be taken into account. Furthermore, approximately one-half of the mice with leukemia had a normal WBC count, thus an analysis of circulating cells also cannot be used alone to determine phenotype. However, enlargement of tissues was a reliable way to grossly define myeloid leukemia. Almost all mice with myeloid disease had a significantly higher-than-normal spleen weight, often presenting with over 10-fold enlargement, while mice with lymphoid leukemia tended to have an enlarged thymus. Flow cytometry was the main method used to define the phenotype of the mice, but was complemented with histology and IHC analyses to avoid misclassification. There were several cases in which the disease appeared to have a clear phenotype by flow but only advanced methods revealed the entire pathology of the animal, such as the L-2 animals, which had a lymphoid pathology with a myeloid surface marker. Thus, M4070 infection can induce multiple and complex phenotypes, which must be carefully scrutinized to make meaningful conclusions about the corresponding CIS-associated genes.

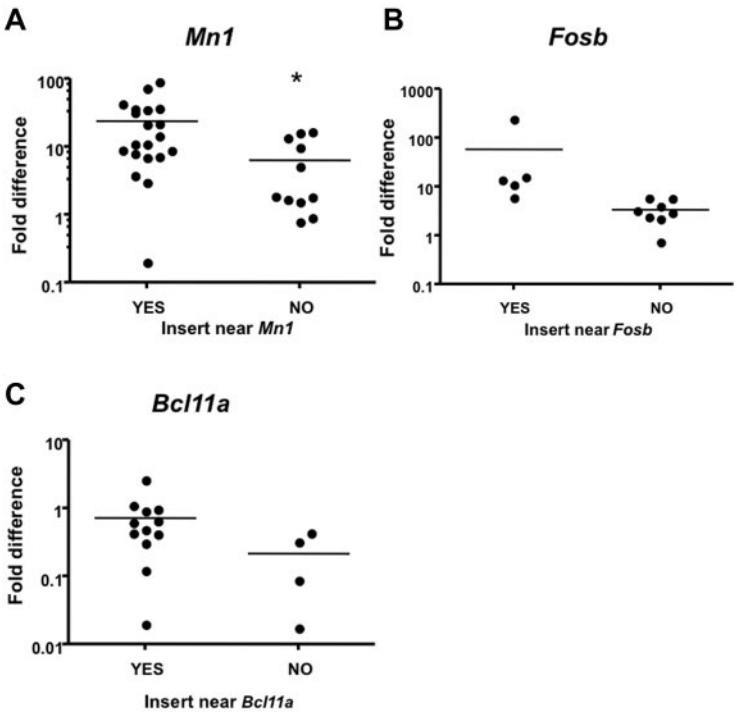

Figure 6. Quantitative real-time PCR analysis indicates higher expression of CIS-associated candidate genes in mice with insertions near those genes. Candidate gene transcript expression in spleens or lymph nodes of mice with insertion events near or away from those genes. Intron-spanning primers were designed. Expression was calculated using the ΔΔCT method[41] and is shown in log scale. Expression level was normalized to the respective WT tissue. Each dot represents one PCR. Reactions were performed on cDNA isolated from leukemia with insertions near other CIS genes labeled with "NO." (A) Reactions performed on cDNA isolated from leukemia with insertions near *Mn1* and the novel gene *C130026L21Rik* labeled with "YES" (*significant *P* value $< .05$). (B) Reactions performed on cDNA isolated from leukemia with insertions near *Fosb* labeled with YES ($P = .153$). (C) Reactions performed on cDNA isolated from leukemia with insertions near *Bcl11a* labeled with YES ($P = .172$).

The use of M4070 to accelerate myeloid leukemia has been established.[14,36] Similarly, we also detected leukemia acceleration in a myeloid leukemia-predisposed background and identified a longer list of CISs, all of which have at least 3 insertions in 3 mice/leukemias. Several candidate genes observed in other MuLV-induced AML models such as *Bcl11a*, *Mn1*, and *Myb* were found in our list. As expected, CIS-associated candidate genes identified almost exclusively in the infected WT cohort presenting with T-cell ALL were known T cell leukemia genes, such as *Ikaros*, *Pim1*, *Notch1*, and *Lmo2*.[25] We also identified candidate genes in this cohort that have not been implicated in lymphoid disease before, such as *Armc2* and *Taf8*. To determine the genes that play an important role in *Mll-AF9* leukemogenesis, the extensive candidate gene list was prioritized by the *Mll-AF9* genotype and myeloid phenotype using Fisher exact tests. This analysis allowed us to narrow the scope of candidate genes we chose for further study. Several candidate genes were found in our screen in *Mll-AF9*–positive myeloid leukemia that had not been reported before and may specifically interact with *Mll-AF9* in leukemogenesis, including *Gimap* genes,[37] *Fosb*, and the novel gene *B230118H07Rik* in the *RAG* locus.[38] However, relatively few CISs were found exclusively in myeloid leukemia from *Mll-AF9* mice. Therefore, we suspect that many of the CIS-associated candidate genes can contribute to myeloid leukemia initiated by *Mll-AF9*, and may also contribute to leukemia formation in other genetic contexts.

Human leukemia databases are important resources to determine whether candidate *Mll-AF9* cooperating mouse genes could be clinically relevant. There was highly variable expression for the 3 top candidate genes (*FOSB, MN1,* and *BCL11A*) among all AML samples, even in the *MLL* rearranged AMLs. There were also many candidate genes that overlapped with the COSMIC[24] or Cancer Gene Census[25] databases (Table 1). These results suggest that *MLL-AF9* likely cooperates with multiple genes, rather than one particularly potent gene, explaining the heterogeneity observed in patients.

Functional tests both in vitro and in vivo were used to provide evidence for a role of *FOSB* or *MN1* in *MLL-AF9* leukemia. *FOSB* is one of 4 genes in the *FOS* gene family thought to be involved in cell processes including proliferation and transformation but has not previously been implicated in AML disease progression. Remarkably, knockdown of *FOSB* expression impaired growth of both human and murine myeloid leukemia cells. These results strongly suggest that *FOSB* is an important novel leukemia gene that cooperates with *MLL-AF9* in our mouse model, becoming a potential therapeutic target for MLL-AF9–driven leukemias. In addition, we show that *MN1* could cooperate in vivo with *Mll-AF9* in myeloid leukemia, postulating that *MN1* may also be an important AML cancer gene depending on the genetic context. These data are consistent with findings that overexpressing *MN1* is sufficient to cause AML in mice.[20] *Mn1* has also been identified as a CIS and cooperator with *NUP98-HOXD13* and *CALM-AF10* in 2 other mouse AML models using this same retrovirus.[14,39] *MN1* has been identified in the Cancer Gene Census database as a known cancer gene and overexpression of *MN1* has been found in both human and mouse AML.[14,20,40] Similarly, *Mn1* insertions were found in leukemic mice induced by a retrovirus encoding *MLL-ENL*. Finally, knockdown of *MN1* can impair growth of myeloid cell lines with *MLL* gene rearrangements and coexpression of *MN1* and *MLL-ENL* with retroviruses can cooperate to induce a rapid AML-like disease.[35]

An important goal of this research was to establish novel *MLL-AF9* cooperating genes that will ultimately lead to new therapeutic strategies for the treatment of AML in patients with this translocation. Some of these are known leukemia genes but their role in *MLL-AF9* leukemia has not been previously reported, such as *MN1,* and some are novel genes that need to be explored, such as *FOSB* and *B230118H07Rik*. Therapeutic targets may also be identified by defining candidate genes from CISs that co-occur, such as *CyclinD2* with *Fosb* and *Sla* or *Pik3cd* in the case of *Mn1* (Figure 4C). Future studies are intended to test drugs on AML cell

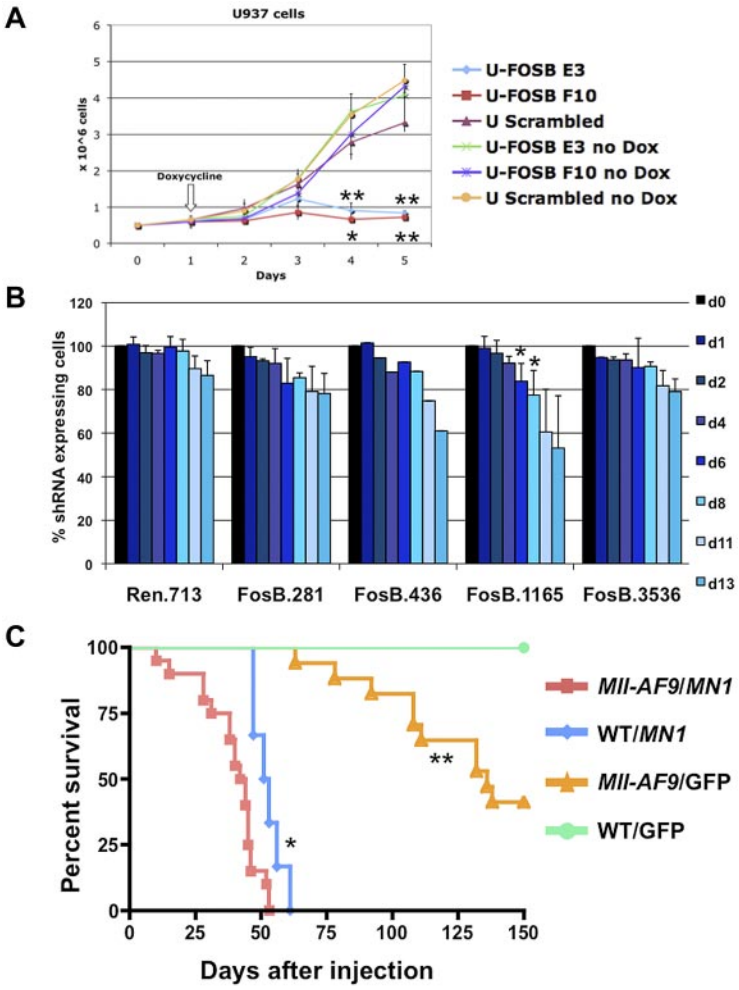

Figure 7. *Fosb* and *Mn1* can contribute to AML maintenance or development of AML with *MLL-AF9*. (A) Growth curve of U937 cells with and without induction of shRNA against *FOSB* with doxycycline. The x-axis represents days after plating cells at 0.5 million cells/well; the y-axis is the number of cells per well in millions of cells. Doxycycline was added 24 hours after plating. Error bars reflect the SD of 3 wells/condition/cell line. Cell lines and conditions were labeled according to the legend (*significant P value $< .05$; **significant P value $< .01$). P values reflect paired t test comparing E3 or F10 shRNA U937 cells to U937 cells with a scrambled control, all treated with doxycycline. (B) shRNA competitive proliferation assay in Tet-On MLL-AF9;Nras^{G12D} AMLs (expressing rtTA3) transduced with indicated TRMPV-Neo-shRNA targeting *Fosb* or *Renilla* luciferase. Cells were drug selected and mixed with 20%-40% untransduced cells, followed by shRNA induction with doxycycline. The percentage of shRNA-expressing cells is monitored over time. Error bars represent 2 or 3 independent experiments except in the case of 436 (*significant P value $< .05$). (C) Kaplan-Meier survival curve of mice injected with BM transduced with a retrovirus containing *MN1* or *GFP*. The x-axis is the number of days after injection of cells into irradiated recipient mice; the y-axis is the percentage of survival. The study was ended at 150 days. Survival of mice receiving *MN1*-transduced *Mll-AF9* BM was significantly shorter than that of mice with *MN1*-transduced WT BM ($P = .0046$) and mice with *GFP*-transduced *Mll-AF9* BM ($P < .0001$); *significant P value $< .001$, **significant P value $< .0001$. A total of 52 mice were used in the study: *Mll-AF9* BM/*MN1* (n = 20), WT BM/*MN1* (n = 6), *Mll-AF9* BM/*GFP* (n = 21), and WT BM/*GFP* (n = 5).

lines and in vivo to serve as preclinical testing for eventual application in human patients with *MLL-AF9* leukemia.

Acknowledgments

The authors thank members of the Largaespada laboratory for insightful discussions. They thank especially Dr Timothy Starr, Dr Vincent Keng, Sue Rathe, Dr Ernesto Diaz-Flores, Jonathan Linehan, Dr Sonja Nodland, Dr Keiko Akagi, Wendy Hudson, Dr Michael Heuser, Dr Bin Yin, Dr Anthony Uren, Dr Mei Lin Maunakea, and Dr Tony Cox for their technical assistance and advice as well as for providing reagents in some cases. They thank the Minnesota Supercomputing Institute for providing computational resources along with systems and database administrative support.

This work was supported by National Cancer Institute grant U01 CA84221 (D.A.L.), the Leukemia & Lymphoma Society of America LLS 7019-04 (D.A.L.), the University of Minnesota Cancer Biology training grant CA009138, and grants from Cancer Research UK and The Wellcome Trust (D.J.A.). S.C.K. is a scholar of the Leukemia & Lymphoma Society. L.S.C. is supported by fellowships from the National Cancer Institute (F32 CA106192 and K01 CA122183) and a postdoctoral fellowship from the American Cancer Society PF-05-153-01.

Authorship

Contribution: R.J.B. designed and performed research, analyzed and interpreted data, prepared figures and legends, and wrote the manuscript; L.S.C. designed and performed research; A.L.S., S.L., M.G.O., and S.C.K. analyzed results and prepared figures and legends; R.A.B., M.D.D., and M.J.N. performed research; J.Z. and A.R.R. performed research, analyzed results, and prepared figures; K.A.T.S., D.F., and A.-F.J.L. analyzed results; L.W. provided reagents; J.H.K. provided reagents and supported research; R.D. and S.W.L. designed research; D.J.A. designed and performed research and contributed to the editing of the manuscript; and D.A.L. designed research, interpreted data, and contributed to writing and editing the manuscript.

Conflict-of-interest disclosure: The authors declare no competing financial interests.

The current affiliation for A.-F.J.L. is Office of the Vice President for Research, University of Minnesota Interdisciplinary Informatics, Minneapolis, MN.

Correspondence: David A. Largaespada, Department of Genetics, Cell Biology and Development, Masonic Cancer Center, University of Minnesota Twin Cities, 6-160 Jackson Hall, 321 Church St, Minneapolis, MN 55455; e-mail: larga002@umn.edu.

References

1. Rowley JD. The role of chromosome translocations in leukemogenesis. *Semin Hematol.* 1999; 36(4 suppl 7):59-72.
2. Felix CA, Kolaris CP, Osheroff N. Topoisomerase II and the etiology of chromosomal translocations. *DNA Repair.* 2006;5(9-10):1093-1108.
3. Daser A, Rabbitts TH. The versatile mixed lineage leukaemia gene MLL and its many associations in leukaemogenesis. *Semin Cancer Biol.* 2005;15(3):175-188.
4. Nakamura T, Alder H, Gu Y, et al. Genes on chromosomes 4, 9, and 19 involved in 11q23 abnormalities in acute leukemia share sequence homology and/or common motifs. *Proc Natl Acad Sci U S A.* 1993;90(10):4631-4635.
5. Huret JL, Senon S, Bernheim A, Dessen P. An Atlas on genes and chromosomes in oncology and haematology. *Cell Mol Biol.* 2004;50(7):805-807.
6. Corral J, Lavenir I, Impey H, et al. An Mll-AF9 fusion gene made by homologous recombination causes acute leukemia in chimeric mice: a method to create fusion oncogenes. *Cell.* 1996; 85(6):853-861.
7. Dobson CL, Warren AJ, Pannell R, et al. The mll-AF9 gene fusion in mice controls myeloproliferation and specifies acute myeloid leukaemogenesis. *EMBO J.* 1999;18(13):3564-3574.
8. Johnson JJ, Chen W, Hudson W, et al. Prenatal and postnatal myeloid cells demonstrate stepwise progression in the pathogenesis of MLL fusion gene leukemia. *Blood.* 2003;101(8):3229-3235.
9. Mikkers H, Berns A. Retroviral insertional mutagenesis: tagging cancer pathways. *Adv Cancer Res.* 2003;88:53-99.
10. Lund AH, Turner G, Trubetskoy A, et al. Genome-wide retroviral insertional tagging of genes involved in cancer in Cdkn2a-deficient mice. *Nat Genet.* 2002;32(1):160-165.
11. Blaydes SM, Kogan SC, Truong BT, et al. Retroviral integration at the Epi1 locus cooperates with Nf1 gene loss in the progression to acute myeloid leukemia. *J Virol.* 2001;75(19):9427-9434.
12. Wolff L, Koller R, Hu X, Anver MR. A Moloney murine leukemia virus-based retrovirus with 4070A long terminal repeat sequences induces a high incidence of myeloid as well as lymphoid neoplasms. *J Virol.* 2003;77(8):4965-4971.
13. Wolff L, Garin MT, Koller R, et al. Hypermethylation of the Ink4b locus in murine myeloid leukemia and increased susceptibility to leukemia in p15(Ink4b)-deficient mice. *Oncogene.* 2003; 22(58):9265-9274.
14. Slape C, Hartung H, Lin YW, Bies J, Wolff L, Aplan PD. Retroviral insertional mutagenesis identifies genes that collaborate with NUP98-HOXD13 during leukemic transformation. *Cancer Res.* 2007;67(11):5148-5155.
15. Starr TK, Allaei R, Silverstein KA, et al. A transposon-based genetic screen in mice identifies genes altered in colorectal cancer. *Science.* 2009;323(5922):1747-1750.
16. Stabenau A, McVicker G, Melsopp C, Proctor G, Clamp M, Birney E. The Ensembl core software libraries. *Genome Res.* 2004;14(5):929-933.
17. Sundstrom C, Nilsson K. Establishment and characterization of a human histiocytic lymphoma cell line (U-937). *Int J Cancer.* 1976;17(5):565-577.
18. Harris P, Ralph P. Human leukemic models of myelomonocytic development: a review of the HL-60 and U937 cell lines. *J Leukoc Biol.* 1985;37(4): 407-422.
19. Zuber J, McJunkin K, Fellmann C, et al. Toolkit for evaluating genes required for proliferation and survival using tetracycline-regulated RNAi. *Nat Biotechnol.* 2011;29(1):79-83.
20. Heuser M, Argiropoulos B, Kuchenbauer F, et al. MN1 overexpression induces acute myeloid leukemia in mice and predicts ATRA resistance in patients with AML. *Blood.* 2007;110(5):1639-1647.
21. Castilla LH, Perrat P, Martinez NJ, et al. Identification of genes that synergize with Cbfb-MYH11 in the pathogenesis of acute myeloid leukemia. *Proc Natl Acad Sci U S A.* 2004;101(14):4924-4929.
22. Ross JA, Robison LL. MLL rearrangements in infant leukemia: is there a higher frequency in females? *Leuk Res.* 1997;21(8):793-795.
23. Akagi K, Suzuki T, Stephens RM, Jenkins NA, Copeland NG. RTCGD: retroviral tagged cancer gene database. *Nucleic Acids Res.* 2004;32(database issue):D523-D527.
24. Forbes SA, Bhamra G, Bamford S, et al. The catalogue of somatic mutations in cancer (COSMIC). *Curr Protoc Hum Genet.* 2008;Chapter 10: Unit 10.11.
25. Futreal PA, Coin L, Marshall M, et al. A census of human cancer genes. *Nat Rev Cancer.* 2004; 4(3):177-183.
26. Valk PJ, Verhaak RG, Beijen MA, et al. Prognostically useful gene-expression profiles in acute myeloid leukemia. *N Engl J Med.* 2004;350(16): 1617-1628.
27. Verhaak RG, Wouters BJ, Erpelinck CA, et al. Prediction of molecular subtypes in acute myeloid leukemia based on gene expression profiling. *Haematologica.* 2009;94(1):131-134.
28. Carella C, Bonten J, Sirma S, et al. MN1 overexpression is an important step in the development of inv(16) AML. *Leukemia.* 2007;21(8):1679-1690.
29. Mullighan CG, Goorha S, Radtke I, et al. Genome-wide analysis of genetic alterations in acute lymphoblastic leukaemia. *Nature.* 2007; 446(7137):758-764.
30. Ferrari S, Torelli U, Selleri L, et al. Study of the levels of expression of two oncogenes, c-myc and c-myb, in acute and chronic leukemias of both lymphoid and myeloid lineage. *Leuk Res.* 1985;9(7):833-842.
31. Wolff L. Myb-induced transformation. *Crit Rev Oncog.* 1996;7(3-4):245-260.
32. Walter MJ, Payton JE, Ries RE, et al. Acquired copy number alterations in adult acute myeloid leukemia genomes. *Proc Natl Acad Sci U S A.* 2009;106(31):12950-12955.
33. Lawrence HJ, Rozenfeld S, Cruz C, et al. Frequent co-expression of the HOXA9 and MEIS1 homeobox genes in human myeloid leukemias. *Leukemia.* 1999;13(12):1993-1999.
34. Sitwala KV, Dandekar MN, Hess JL. HOX proteins and leukemia. *Int J Clin Exp Pathol.* 2008; 1(6):461-474.
35. Liu T, Jankovic D, Brault L, et al. Functional characterization of high levels of meningioma 1 as collaborating oncogene in acute leukemia. *Leukemia.* 2010;24(3):601-612.
36. Wolff L, Garin MT, Koller R, et al. A novel retrovirus provides the cooperating oncogenic event(s) required to demonstrate the tumor suppressor activity of p15Ink4b in myeloid cells in vivo. *Blood Cells Mol Dis.* 2004;32(1):226-231.
37. Nitta T, Takahama Y. The lymphocyte guard-IANs: regulation of lymphocyte survival by IAN/GIMAP family proteins. *Trends Immunol.* 2007;28(2):58-65.
38. Cebrat M, Miazek A, Kisielow P. Identification of a third evolutionarily conserved gene within the RAG locus and its RAG1-dependent and -independent regulation. *Eur J Immunol.* 2005;35(7): 2230-2238.
39. Caudell D, Harper DP, Novak RL, et al. Retroviral insertional mutagenesis identifies Zeb2 activation as a novel leukemogenic collaborating event in CALM-AF10 transgenic mice. *Blood.* 2010; 115(6):1194-1203.
40. Grosveld GC. MN1, a novel player in human AML. *Blood Cells Mol Dis.* 2007;39(3):336-339.
41. Livak KJ, Schmittgen TD. Analysis of relative gene expression data using real-time quantitative PCR and the 2(-Delta Delta C(T)) method. *Methods.* 2001;25(4):402-408.